Journal of Physical Organic Chemistry

WILEY

Journal of Physical Organic Chemistry

RESEARCH ARTICLE OPEN ACCESS

Tetra(4-hexylphenyl) [3]- and [5]Cumulenes

Bozheng Sun[1] | Stefano Pecorario[2] | Elda Sala[3,4] | Mario Caironi[3] | Michael J. Ferguson[1] | Carlo S. Casari[4] | Rik R. Tykwinski[1]

[1]Department of Chemistry, University of Alberta, Edmonton, Alberta, Canada | [2]Cavendish Laboratory, University of Cambridge, Cambridge, UK | [3]Center for Nano Science and Technology, Istituto Italiano di Tecnologia, Milan, Italy | [4]Department of Energy, Politecnico di Milano, Micro and Nanostructured Materials Lab NanoLab, Milan, Italy

Correspondence: Rik R. Tykwinski (rik.tykwinski@ualberta.ca)

Received: 13 March 2025 | **Revised:** 23 March 2025 | **Accepted:** 29 March 2025

Funding: This work was supported by Natural Sciences and Engineering Research Council of Canada (2017-05052 and RGPIN-2023-04000) and Canada Foundation for Innovation, and Polifab.

Keywords: cumulene | cumulene stability | film formation | organic field effect transistor | radialene

ABSTRACT

The synthesis of [3]- and [5]cumulenes bearing 4-hexylphenyl endgroups, **[3]PhHex** and **[5]PhHex**, has been developed. The incorporation of alkyl groups is designed to enhance film formation by improving solubility. Although tetraaryl[3]cumulenes are typically quite stable, the head-to-tail dimerization of **[3]PhHex** is observed after prolonged storage under ambient conditions, and the dimer is characterized crystallographically. The crystallographic analysis of **[5]PhHex** in comparison with other tetraaryl[5]cumulenes demonstrates changes in packing as a function of increasing size of the alkyl group. Preliminary characterization of field-effect transistors fabricated with **[3]PhHex**, in comparison with the parent compound tetraphenyl[3]cumulene **[3]Ph**, shows poorer performance for **[3]PhHex** and emphasizes the need to optimize film-forming protocols for new cumulenic semiconductors.

1 | Introduction

Conjugated organic molecules offer substantial opportunities as organic semi-conducting materials as a result of delocalized, polarizable π-electrons. The field of organic materials is largely dominated by aromatic and heteroaromatic molecules, particularly acenes [1, 2]. On the other hand, hydrocarbon molecules with unique π-structures based on sp-hybridized carbon have been suggested as strong candidates for future electronic materials, including, for example, oligoynes/polyynes [3–8], polydiacetylenes [9], graphynes [10], and, as the focus of the this study, [*n*]cumulenes [11–14]. For example, field-effect transistors (FETs) based on [3]Ph (Figure 1) have been investigated and reported as a promising component in molecular devices [15, 16]. As is typically observed for organic molecules with π-rich systems such as acenes [1, 2], [3]Ph exhibits p-type behavior due to its delocalized HOMO, while its high LUMO energy hinders electron injection. Recently, [3]Ph has also been embedded into a polymer as the active component of a supercapacitor [17].

As with most of conjugated small molecules, the fabrication of electronic devices using [3]Ph as the semiconducting layer can suffer from poor and non-uniform film coverage when deposited by drop-casting, due to the formation of needle-like microcrystals. Consequently, low charge mobilities [2×10^{-3} cm^2/(V s)] were observed in first-generation field-effect transistors (FETs) [15]. On the other hand, specialized techniques can drastically improve performance. For example, the controlled deposition of [3]Ph films using a wire-bar coating technique has been developed to improve uniformity and microcrystalline order, leading to increased charge mobilities up to 0.1 cm^2/(V s) [16].

Given the typical challenges encountered with casting of films with small molecules, a method for producing homogeneous

films would be desirable to facilitate the exploration of the potential of [*n*]cumulenes as semiconductors. Beyond optimizing deposition techniques for each new [*n*]cumulene, substitution with aliphatic groups offers the prospect to modify crystal morphology, increase the solubility, and improve the processability from solution [18–20]. Thus, it was hypothesized that introducing aliphatic substituents on the endgroups of an [*n*]cumulene could improve the quality of solution-cast films.

As little is known about *n*-alkyl substituted [3]- or [5]cumulenes (a singular example, 4-ethyl-tetrapheny[5]cumulene [5]PhEt, has been reported [21]), the inclusion of *n*-hexyl groups has been selected as a starting point. These groups are considered sufficiently large to improve the solubility and processability without undermining the intermolecular communication of the [*n*]cumulenes necessary for charge transport. The corresponding [3]cumulene, [3]PhHex, is targeted for comparison with the previously reported results using [3]Ph as a semiconductor. The energy of the HOMO in [*n*]cumulenes is known to increase as a function of length of the sp-backbone [22], and the next longer homolog, [5]PhHex, is targeted to examine the relationship between the length of [*n*]cumulenes and electronic/structural characteristics. We report herein the synthesis, spectroscopic analysis, and physical characterization of [3]PhHex and [5]PhHex, as well as preliminary device data (OFETs) for [3]PhHex.

2 | Synthesis of [3]PhHex and [5]PhHex

The synthesis of [*n*]cumulenes bearing 4-hexylphenyl endgroups started with the formation of di-(4-*n*-hexylphenyl)methanol **1** (Scheme 1a) [23]. 4-*n*-Hexylphenyl bromide was converted into the Grignard reagent and reacted immediately with ethyl formate to afford alcohol **1** in 81% yield. Oxidation of compound **1** with PCC gave diaryl ketone **2**. Lithium trimethylsilylacetylide, generated from trimethylsilylacetylene, reacted with ketone **2**, followed by quenching with methyl iodide to afford compound **3** in 95% yield. Desilylation of **3** with K_2CO_3 in MeOH afforded the terminal alkyne **4**, which is a benchtop-stable oil, in a yield of 96%. Terminal alkyne **4** was converted to the lithium acetylide via deprotonation with *n*BuLi, and the subsequent reaction with ketone **2** followed by *O*-methylation of the intermediate alkoxide with methyl iodide afforded compound **5** in 72% yield. The reductive elimination [24] of **5** was carried out with $SnCl_2$ in the presence of catalytic HCl and afforded **[3]PhHex** as a yellow, amorphous solid in 84%. During attempts to produce X-ray quality crystals, a solution of **[3]PhHex** CH_2Cl_2/MeOH was left to stand for several weeks under ambient conditions without protection from light, which produced a light-yellow crystal. Crystallographic analysis of this crystal (vide infra) revealed the structure of the dimeric product **6** (Scheme 1a). Several attempts to reproduce the formation of **6** on a larger scale under similar conditions were, however, unsuccessful, preventing further spectroscopic characterization. In view of the known formation of analogous dimers (see crystallographic studies below), the formation of **6** was not further pursued.

The synthesis of **[5]PhHex** utilized terminal alkyne **4** in an oxidative acetylenic Hay coupling reaction [25] affording diether **7** in 94% yield (Scheme 1b). The reductive elimination of **7** using $SnCl_2$ and HCl to form **[5]PhHex**, however, was initially unsuccessful when using CH_2Cl_2 as the solvent. A mixture of red, needle-like crystals (presumably the desired product **[5]PhHex**) were formed during the precipitation process along with a deep red, greasy oil that prevented efficient purification. The ^{1}H NMR spectrum of this mixture displayed a number of broadened signals, in addition to the well-resolved signals corresponding to **[5]PhHex**. Thus, the reductive elimination reaction was explored in alternative solvents (THF and Et_2O) and at lower temperature (0°C). Ultimately, the reaction in THF at room temperature afforded pure **[5]PhHex** as a bright red, crystalline solid in 68% yield. The isolated, pure cumulene **[5]PhHex** is stable at room temperature for months, as confirmed by TLC and ^{1}H NMR analyses.

It is worth emphasizing that a more direct route to **[5]PhHex**, commonly used for the synthesis of [*n*]cumulenes, would use the alcohol **8** without formation of the methyl ether (Scheme 2).

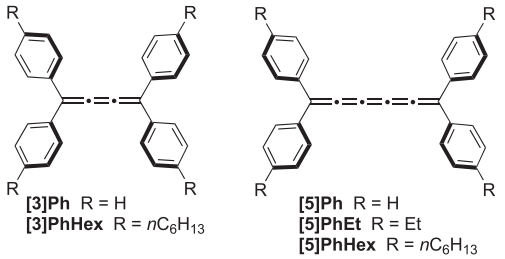

FIGURE 1 | [*n*]Cumulenes discussed in this manuscript.

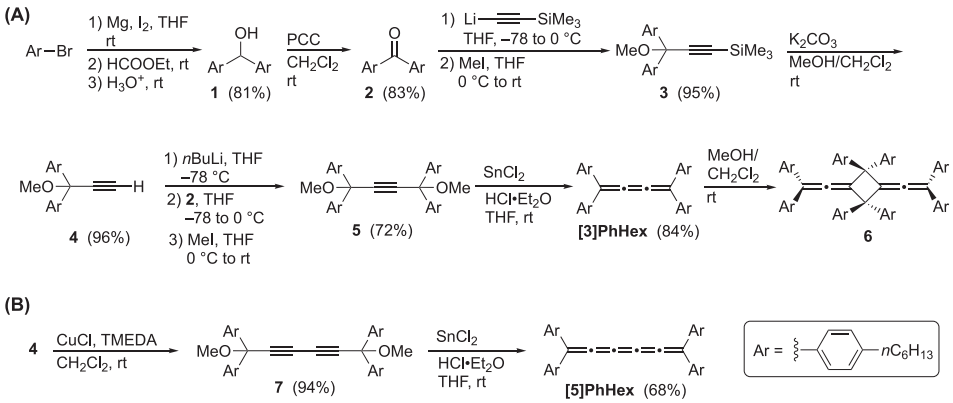

SCHEME 1 | Synthesis of **[3]**- and **[5]PhHex**.

Unfortunately, attempts to execute this approach were unsuccessful. The alcohol **8** was obtained without problems, and desilylation of **8** with K_2CO_3/MeOH appeared to proceed normally to give **9**. For unknown reasons, however, the terminal alkyne proved unstable, and storing **9** led to gradual decomposition as observed by TLC analysis. Due to this instability, this route was not further pursued.

3 | Crystallographic Studies

Given the relationship(s) between crystalline morphology and device performance in OFETs, it was highly desirable to compare the solid-state packing of **[3]PhHex** with that of **[3]Ph** [26]. Attempts to produce a single crystal of **[3]PhHex** suitable for crystallographic analysis were, unfortunately, unsuccessful under various conditions (e.g., CH_2Cl_2/MeOH, $CHCl_3$/MeOH, CH_2Cl_2/EtOH, toluene/MeOH; −20°C or room temperature). Instead, crystallization predominantly afforded a deep yellow, amorphous solid of pure **[3]PhHex**. In one case, a solution of **[3]PhHex** in CH_2Cl_2/MeOH was left to stand for several weeks under ambient conditions, resulting in a light-yellow crystal. Crystallographic analysis confirmed the head-to-tail structure of **6** (Figure 2a). The conversion of [3]cumulenes to dimeric derivatives is known, and crystallographic analysis has been reported for other head-to-tail dimers [27–29] similar to **6** (Figures 2b–d), as well as head-to-head [30] and symmetrical dimers [28, 31].

A single crystal of **[5]PhHex** suitable for crystallographic studies was acquired by diffusion of MeOH into a solution of CH_2Cl_2 at room temperature (Figure 3). The bond angles of the cumulenic moiety, at 177.4° and 179.1°, confirm the linearity of the sp-chain. The conformations of the alkyl chains in **[5]PhHex** are well ordered, and the C—C bonds of the alkyl groups assume a staggered conformation.

Bond length alteration (BLA = the difference between long and short carbon–carbon bonds) is a valuable parameter to

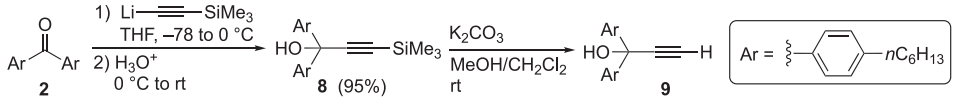

SCHEME 2 | Synthesis toward propargyl alcohol **9**.

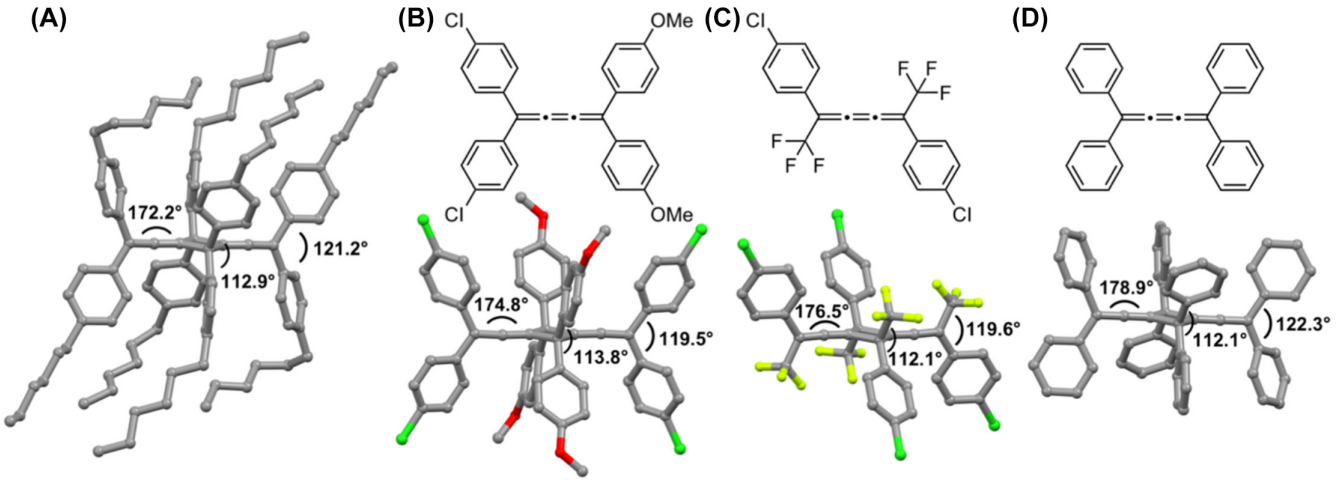

FIGURE 2 | Crystal structures and selected bond angles for head-to-tail dimers from [3]cumulenes: Dimers of (a) **[3]PhHex** (compound **6**), (b) 1,1-bis(4-chlorophenyl)-4,4-bis(4-methoxyphenyl)butatriene [27], (c) 1,4-bis(4-chlorophenyl)-1,4-bis(trifluromethyl)butatriene [28], and (d) **[3]Ph** [29]. Hydrogen atoms are removed for clarity.

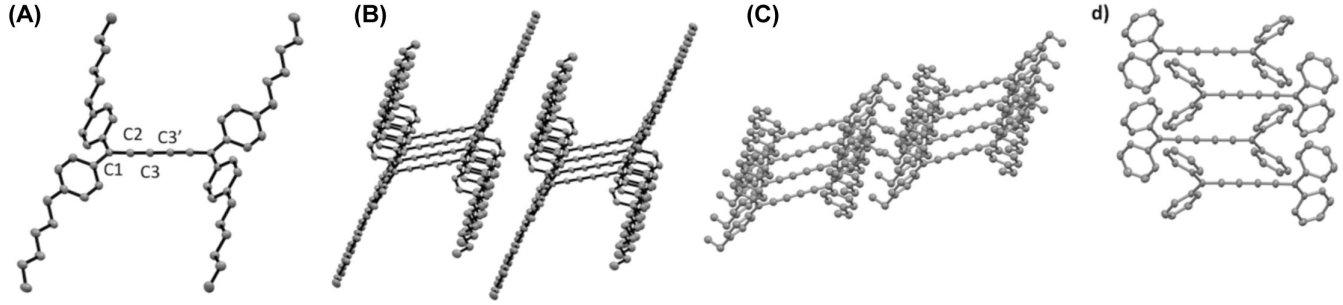

FIGURE 3 | (a) Crystal structure of **[5]PhHex** (ellipsoids are shown at 50% probability level; H-atoms are omitted for clarity). Selected bond angles [°] and lengths [Å]: C1—C2 1.347(2), C2—C3 1.256(2) C3—C3′ 1.306(3); C1—C2—C3 177.44(17) C2—C3—C3′ 179.1(2). (b) Crystal packing of **[5]PhHex**. (c) Crystal packing of **[5]PhEt** [32]. (d) Crystal packing of **[5]Ph**.

examine the structural and electronic characterization of conjugated molecules. BLA for polyynes remains quite strong, ranging from 0.16 Å (a triyne) to a limiting value of approximately 0.14 Å for the longest polyynes [33]. In contrast, BLA is significantly lower of cumulenes and has been strongly correlated to the semiconducting behavior of the cumulenic moiety [13, 34]. For **[5]PhHex**, the BLA is 0.050 Å [35], which is consistent with other known [5]cumulenes, including 0.048 Å for **[5]Mes** (Mes = mesityl), 0.059 Å for **[5]PhEt**, and 0.058 Å for **[5]Ph** [17].

Cumulene **[5]PhHex** shows a parallel-displaced orientation (Figures 3a,b) in the solid state, offset along the longitudinal axis of the cumulenic moiety. The closest intermolecular distance separating cumulenic moieties for **[5]PhHex** is 6.1 Å, which is larger than 5.6 Å in **[5]PhEt** (Figure 3c) and 3.9 Å in **[5]Ph** (Figures 3c,d). The packing of **[5]PhHex** is dominated by C-H–π interactions between neighboring aryl groups and alkyl-alkyl interactions. This packing motif places one of the aryl rings over the core of the cumulenes, providing the shortest interatomic distance between neighboring molecules at ca. 3.6 Å (see Figure S1). Thus, while the intermolecular π-orbital overlap in the crystal of **[5]PhHex** is far from ideal, communication may be maintained through contact between the aromatic endgroup and the cumulenic moieties.

4 | UV–Vis Spectroscopic Studies

The UV–vis spectra of **[3]PhHex** and **[5]PhHex** have been measured in CH_2Cl_2 and are shown in comparison to **[3]Ph** and **[5]Ph** (Figure 4). Overall, the spectra show spectral characteristics similar to those of other [3]- and [5]cumulenes reported in the literature regarding their band shapes and absorption wavelengths (λ), particularly in terms of the lowest energy absorption wavelength λ_{max} [36]. Compared with **[3]Ph** (λ_{max} = 420 nm) and **[5]Ph** (λ_{max} = 486 nm) [37, 38], substitution with electron-donating alkyl groups has produced a redshift of the λ_{max} of 16 nm for **[3]PhHex** (λ_{max} = 436 nm) and 20 nm for **[5]PhHex** (λ_{max} = 506 nm). The most noticeable effect of adding alkyl substituents is the increased molar absorptivity, particularly for **[5]PhHex** (ε = 82,000). The spectra of **[3]PhHex** and **[3]Ph** were compared as thin films cast from 1,2-dichlorobenzene (see SI for details). For both [3]cumulenes, the lowest energy transition is split into two distinct absorptions, accompanied by red shifts in the absorptions versus solution values (**[3]PhHex** λ = 458 and 436 nm and **[3]Ph** λ = 452 and 422 nm).

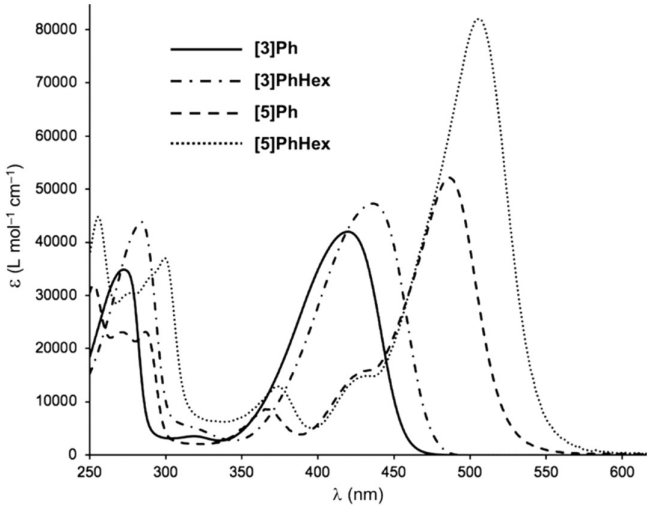

FIGURE 4 | UV–vis spectra of **[3]Ph**, **[3]PhHex**, **[5]Ph**, and **[5]PhHex** (measured in CH_2Cl_2).

5 | Thermal Analyses

The thermal analyses of **[3]PhHex** and **[5]PhHex** have been measured via differential scanning calorimetry (DSC) in comparison with **[3]Ph** and **[5]Ph**. The parent cumulene **[3]Ph** shows a melting point at 242°C, which is immediately followed by decomposition at 243°C [15]. The melting point of **[3]PhHex** (113°C) is significantly lower than that of **[3]Ph**, and **[3]PhHex** is stable as a liquid up to the onset of its decomposition point of 219°C (the decomposition spans from 219 to 300°C; Figure S21). While not within the scope of the presented study, the stability of **[3]PhHex** beyond its melting point may facilitate improved films via annealing [39] or offer an alternative method for the formation of semiconducting films via a melt [40]. The [5]cumulene **[5]PhHex** shows a clear melting point at 74°C, and melting is followed immediately by the onset of broad thermal decomposition at 78°C (peak 96°C; Figure S22). The decomposition point of **[5]PhHex** is substantially lower than that of **[5]Ph** (183°C, Figure S21) [41–44].

6 | Fabrication of Devices Using [3]PhHex

The electronic properties of **[3]PhHex** have been evaluated in the form of thin films by assessing charge-transport in a proof-of-concept FET. The FET was assembled with a top-gate bottom-contact architecture, adopting a thin film of **[3]PhHex** as the semiconducting layer. The layer of **[3]PhHex** was deposited by wire-bar coating at 100°C from a solution *ortho*-dichlorobenzene (10 g/L) and with a bar-speed of 30 mm/s, achieving a film thickness of about 20 nm [45, 46]. The dielectric layer was formed by depositing a 345 nm thick film of parylene C on top of the semiconductor, followed by inkjet printing of an 80 nm-thick poly(3,4-ethylenedioxythiophene) polystyrene sulfonate (PEDOT:PSS) gate electrode (Figure 5a).

The proof-of-concept FET device was studied for its transfer characteristics in the linear (V_{ds} = −5 V) and the saturation (V_{ds} = −40 V) regimes. The results clearly show *p*-type field effect behavior with enhanced I_d in the region of $V_{gs} < 0$ and an on–off currents ratio of 10^4 (Figure 5b). In the **[3]PhHex** device, the subthreshold slope is shallow, and the threshold voltage can be approximated at −0.5 V and −16.5 V for the linear and saturation regimes, respectively. A slight hysteresis of I_d is observed, especially in the saturation regime. In addition, a significant gate leakage current (I_g) is present. Given the lack of ideality in the transfer curves, the field-effect hole mobility (μ) of this device can only be estimated at ca. 10^{-4} cm^2 V^{-1} s^{-1}, with a clear gate dependence across the entire V_g sweep (Figure S2).

The FET results establishes the possibility of adopting a thin film of **[3]PhHex** as a semiconducting material, similar to **[3]Ph**, but with poorer electrical performances [15, 16].

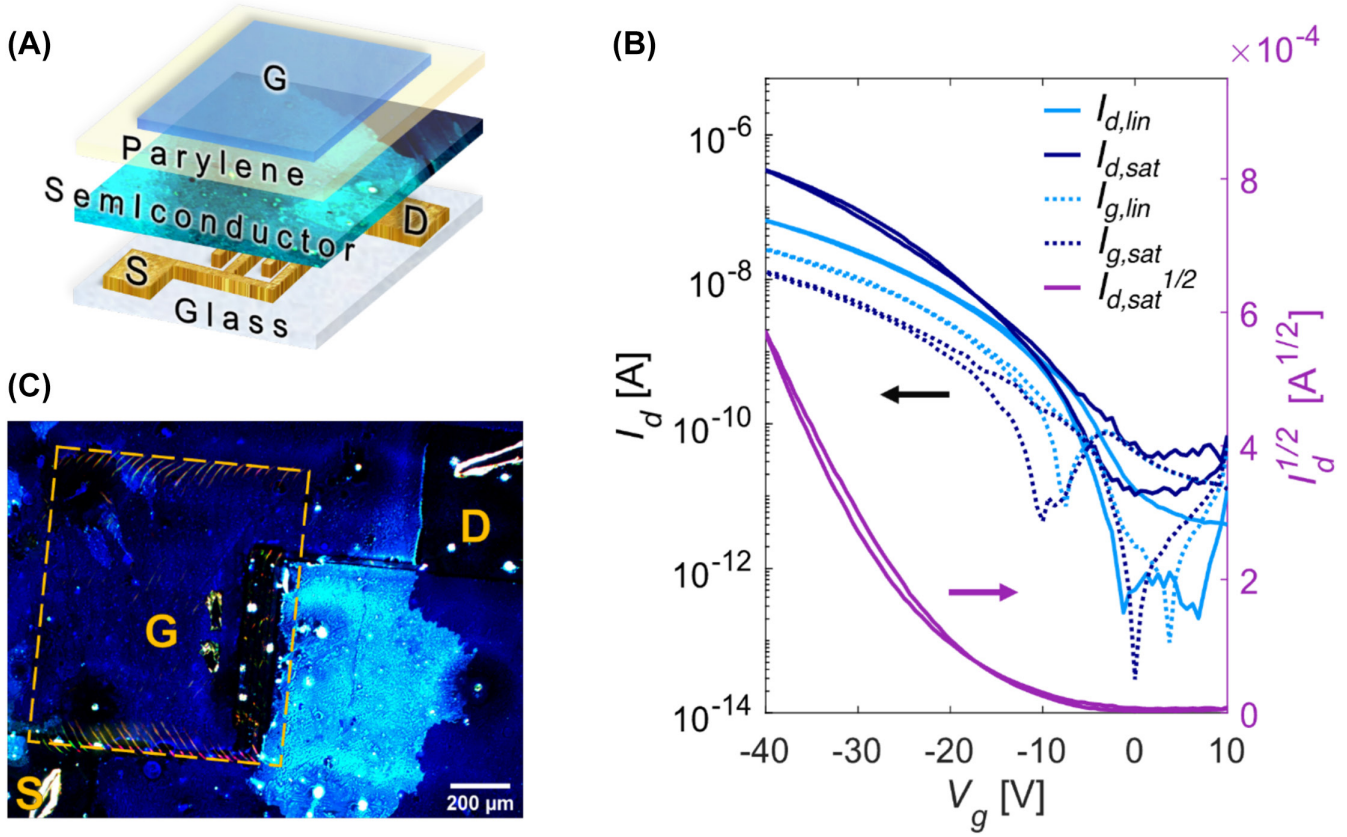

FIGURE 5 | (a) Device architecture of a top-gate bottom-contact FET fabricated with **[3]PhHex**; S, D, and G represent source, drain, and gate electrodes, respectively. (b) Representative transfer characteristic curves of the transistor ($L = 2.5\,\mu m$; $W = 2\,mm$) based on **[3]PhHex**. The drain current (I_d, solid lines) and the gate leakage current (I_g, dashed lines) in the linear ($V_{ds} = -5\,V$) and saturation ($V_{ds} = -40\,V$) regimes are shown in a logarithmic scale. The I_d is plotted in a square root scale for the saturation regime (purple line). (c) Polarized optical microscopy image of the transistor (polarization angle = 90°), with S, D, and G being the device terminals depicted in (a).

Polarized optical microscopy shows that crystalline domains of **[3]PhHex** are very large (Figure 5c and Figure S1), and comparable in size to those obtained for **[3]Ph**, when deposited at similar temperatures [15]. However, the microstructure of such **[3]PhHex** films displays charge-hindering defects, such as cracks and a lack of uniformity. Such non-optimal film morphology can, in part, explain the poor electronic performances of **[3]PhHex**. While future efforts to obtain more ideal morphologies may lead to improved charge transport in **[3]PhHex** films, it is important to note that findings reported here regarding the comparative molecular packing of **[5]PhHex** and **[5]Ph** suggest weaker electronic overlap between adjacent **[3]PhHex** with respect to **[3]Ph**, possibly indicating a fundamental limit [15, 16]. Overall, this study proves that cumulenes solid state packing can be strongly affected by side-chain engineering, without altering the excellent conjugation of the sp-cumulenic chain. Future research directions might explore other strategies to improve the electronic coupling in solid state, such as promoting Herringbone packing.

7 | Conclusions

A new endgroup, namely the 4-*n*-hexylphenyl group, has been developed for the functionalization of a [3]- and [5]cumulene, **[3]PhHex** and **[5]PhHex**, in order to explore the formation of more uniform crystalline films in FET devices. The UV–vis spectra of **[3]PhHex** and **[5]PhHex** exhibit red shifts of the absorption wavelengths compared to the parent compounds **[3]Ph** and **[5]Ph** due to the electron-donating alkyl substituents. While **[3]PhHex** does not form X-ray quality crystals, the formation of a head-to-tail dimer **6** has been identified from a solution of **[3]PhHex** stored at room temperature. The crystal structure of **[5]PhHex** reveals ordered stacking of hexyl groups, resulting in the parallel alignment of neighboring cumulenes at a distance of ca. 6 Å. A proof-of-concept FET device has been fabricated with **[3]PhHex**. The device shows *p*-type semiconducting character, but film quality and charge-carrier mobilities are poor (ca. $10^{-4}\,cm^2V^{-1}s^{-1}$). Thus, further design refinement, structural optimization, and improved film formation are necessary to optimize the electrical properties of [*n*]cumulenes as semiconductors.

Acknowledgments

R.R.T. acknowledges funding from the Natural Sciences and Engineering Research of Canada (NSERC, grants no. RGPIN-2017-05052 and RGPIN-2023-04000) and the Canada Foundation for Innovation (CFI). Part of this work was carried out at Polifab, the micro and nanotechnology center of the Politecnico di Milano.

Data Availability Statement

The data that supports the findings of this study are available in the supplementary material of this article

References

1. J. E. Anthony, "Functionalized Acenes and Heteroarenes for Organic Electronics," *Chemical Reviews* 106 (2006): 5028–5048.

2. J. E. Anthony, "The Larger Acenes: Versatile Organic Semiconductors," *Angewandte Chemie, International Edition* 47 (2008): 452–483.

3. M. R. Bryce, "A Review of Functional Linear Carbon Chains (Oligoynes, Polyynes, Cumulenes) and Their Applications as Molecular Wires in Molecular Electronics and Optoelectronics," *Journal of Materials Chemistry C* 9 (2021): 10524–10546.

4. A. Milani, M. Tommasini, V. Barbieri, et al., "Semiconductor-to-Metal Transition in Carbon-Atom Wires Driven by sp2 Conjugated End Groups," *Journal of Physical Chemistry C* 121 (2017): 10562–10570.

5. V. I. Artyukhov, M. Liu, and B. I. Yakobson, "Mechanically Induced Metal–Insulator Transition in Carbyne," *Nano Letters* 14 (2014): 4224–4229.

6. C. S. Casari and A. Milani, "Carbyne: From the Elusive Allotrope to Stable Carbon Atom Wires," *MRS Communications* 8 (2018): 207–219.

7. S. Kutrovskaya, A. Osipov, S. Baryshev, et al., "Excitonic Fine Structure in Emission of Linear Carbon Chains," *Nano Letters* 20 (2020): 6502–6509.

8. C. S. Casari, M. Tommasini, R. R. Tykwinski, and A. Milani, "Carbon-Atom Wires: 1-D Systems With Tunable Properties," *Nanoscale* 8 (2016): 4414–4435.

9. F. Fang, F. Meng, and L. Luo, "Recent Advances on Polydiacetylene-Based Smart Materials for Biomedical Applications," *Materials Chemistry Frontiers* 4 (2020): 1089–1104.

10. D. Malko, C. Neiss, F. Viñes, and A. Görling, "Competition for Graphene: Graphynes With Direction-Dependent Dirac Cones," *Physical Review Letters* 108 (2012): 086804.

11. A. Konishi, S. Imai, S. Satake, K. Chiba, and M. Yasuda, "Synthesis and Characterization of Hexafluorocyclopentane-Bridged Bisbutatrienes as Models for Longer Cumulenes: Various Transformations for the Construction of π-Conjugated Frameworks," *Chemistry - A European Journal* 29 (2023): e202301255.

12. Y. Hirao, Y. Daifuku, K. Ihara, and T. Kubo, "Spin–Spin Interactions in One-Dimensional Assemblies of a Cumulene-Based Singlet Biradical," *Angewandte Chemie, International Edition* 60 (2021): 21319–21326.

13. M. H. Garner, W. Bro-Jørgensen, P. D. Pedersen, and G. C. Solomon, "Reverse Bond-Length Alternation in Cumulenes: Candidates for Increasing Electronic Transmission With Length," *Journal of Materials Chemistry C* 122, no. 47 (2018): 26777–26789.

14. D. Bain, J. Chang, Y. Lai, T. Khazanov, P. J. Milner, and A. J. Musser, "Torsional Disorder in Tetraphenyl [3]-Cumulenes: Insight Into Excited State Quenching," *Photochemistry* 4 (2024): 138–150.

15. A. D. Scaccabarozzi, A. Milani, S. Peggiani, et al., "A Field-Effect Transistor Based on Cumulenic sp-Carbon Atomic Wires," *Journal of Physical Chemistry Letters* 11 (2020): 1970–1974.

16. S. Pecorario, A. D. Scaccabarozzi, D. Fazzi, et al., "Stable and Solution-Processable Cumulenic sp-Carbon Wires: A New Paradigm for Organic Electronics," *Advanced Materials* 34 (2022): 2110468.

17. S. Ghosh, M. Righi, S. Melesi, Y. Qiu, R. R. Tykwinski, and C. S. Casari, "Cumulenic sp-Carbon Atomic Wires Wrapped With Polymer for Supercapacitor Application," *Carbon* 234 (2024): 119952.

18. M. Klues and G. Witte, "Crystalline Packing in Pentacene-Like Organic Semiconductors," *CrystEngComm* 20 (2018): 63–74.

19. S. M. Ryno, C. Risko, and J.-L. Brédas, "Impact of Molecular Packing on Electronic Polarization in Organic Crystals: The Case of Pentacene vs TIPS-Pentacene," *Journal of the American Chemical Society* 136 (2014): 6421–6427.

20. D. Wasserfallen, M. Kastler, W. Pisula, et al., "Suppressing Aggregation in a Large Polycyclic Aromatic Hydrocarbon," *Journal of the American Chemical Society* 128 (2006): 1334–1339.

21. N. Suzuki, N. Ohara, K. Nishimura, et al., "Characterization of the E Isomer of Tetrasubstituted [5]Cumulene and Trapping of the Z Isomer as a Zirconocene Complex," *Organometallics* 30 (2011): 3544–3548.

22. J. A. Januszewski, D. Wendinger, C. D. Methfessel, F. Hampel, and R. R. Tykwinski, "Synthesis and Structure of Tetraarylcumulenes: Characterization of Bond-Length Alternation Versus Molecule Length," *Angewandte Chemie, International Edition* 52 (2013): 1817–1821.

23. Compound **1** has been reported from a different synthetic method and limited characterization, see Muraoka, M.; Itoh, T.; Mizuma, T.; Toyoshima, S. Researches on Chemotherapeutic Drugs against Viruses. XXX. Synthesis and Antiviral Activity of 2-Dimethylaminoethyl Alkylbenzhydryl Ether. *Chem. Pharm. Bull*. **1960**, *8*, 860–866.

24. J. L. Marshall, D. Lehnherr, B. D. Lindner, and R. R. Tykwinski, "Reductive Aromatization/Dearomatization and Elimination Reactions to Access Conjugated Polycyclic Hydrocarbons, Heteroacenes, and Cumulenes," *ChemPlusChem* 82 (2017): 967–1001.

25. A. S. Hay, "Oxidative Coupling of Acetylenes. II," *Journal of Organic Chemistry* 27 (1962): 3320–3321.

26. Z. Berkovitch-Yellin and L. Leiserowitz, "Electron Density Distribution in Cumulenes: An X-Ray Study of Tetraphenylbutatriene at 20°C and −160°C," *Acta Crystallographica Section B* 33 (1977): 3657–3669.

27. S. Ueta, K. Hida, M. Nishiuchi, and Y. Kawamura, "Regioisomeric Allene Dimer Formation by the Reaction of Tetraarylbutatrienes With Tetracyanoethene," *Organic & Biomolecular Chemistry* 12 (2014): 2784–2791.

28. H. Uno, K. Kasahara, N. Nibu, S. Nagaoka, and N. Ono, "Thermal and Photochemical Isomerization of Tetraaryl Tetrakis(trifluoromethyl) 4 Radialenes," *Journal of Organic Chemistry* 65 (2000): 1615–1622.

29. Z. Berkovitch-Yellin, M. Lahav, and L. Leiserowitz, "Photochemistry of Crystalline Cumulenes. Reassignment of the Structure of the Solid-State Photodimer of Tetraphenylbutatriene," *Journal of the American Chemical Society* 96 (1974): 918–920.

30. M. Kaftory, I. Agmon, M. Ladika, and P. J. Stang, "X-Ray Structure Determination and Mechanism of Formation of two Unique Cumulene Cyclodimers," *Journal of the American Chemical Society* 109 (1987): 782–787.

31. F. W. Nader, C.-D. Wacker, H. Irngartinger, U. Huber-Patz, R. Jahn, and H. Rodewald, "On the Thermal Behavior of Butatrienecarboxylic Acid Derivatives: Crystal and Molecular Structure of a [4]Radialene Tetracarboxylic Ester," *Angewandte Chemie, International Edition* 24 (1985): 852–853.

32. N. Suzuki, D. Hashizume, and T. Chihara, "1,1,6,6-Tetrakis(4-ethylphenyl)-1,2,3,4,5-Hexapentaene," *Acta Crystallographica Section E* 63 (2007): o3436.

33. Y. Gao and R. R. Tykwinski, "Advances in Polyynes to Model Carbyne," *Accounts of Chemical Research* 55 (2022): 3616–3630.

34. M. H. Garner, W. Bro-Jørgensen, and G. C. Solomon, "Three Distinct Torsion Profiles of Electronic Transmission Through Linear Carbon Wires," *Journal of Materials Chemistry C* 124 (2020): 18968–18982.

35. As calculated as the difference in bond lengths of the two central-most bonds in the cumulene chain.

36. D. Wendinger and R. R. Tykwinski, "Odd [n]Cumulenes (N = 3, 5, 7, 9): Synthesis, Characterization, and Reactivity," *Accounts of Chemical Research* 50 (2017): 1468–1479.

37. J. L. Marshall, F. Arslan, J. A. Januszewski, M. J. Ferguson, and R. R. Tykwinski, "A Tetraethynyl [5]Cumulene," *Helvetica Chimica Acta* 102 (2019): e1900001.

38. H. Fischer, *The Chemistry of Alkenes*, ed. S. Patai (New York: John Wiley & Sons Ltd., 1964): 1025–1159.

39. J. Mei, Y. Diao, A. L. Appleton, L. Fang, and Z. Bao, "Integrated Materials Design of Organic Semiconductors for Field-Effect Transistors," *Journal of the American Chemical Society* 135 (2013): 6724–6746.

40. R. Enomoto and Y. Murakami, "Solvent-Free Temperature Gradient Melt Formation of Efficient Visible-to-UV Photon Upconversion Organic Films With Subsolar Threshold and Over 100 h Photostability in Air," *Journal of Materials Chemistry C* 11 (2023): 1678–1683.

41. There is some discrepancy in the values reported for the melting point of **[5]Ph**. The original synthetic report gave the mp as 298°C (ref 41), Kuwatani et al. report >250°C (ref 42), while Islam et al. report 148°C–149°C (ref 43). The di- and trimerization of **[5]Ph** is known,[42,43] and may affect these measurements. Our own DSC analysis does not show an endotherm consistent with melting. An exothermic event, i.e., decomposition, is observed with an onset of 183°C and a peak at 187°C (see Figure S23 for DSC trace).

42. W. Ried, W. Schlegelmilch, and S. Piesch, "Äthinierungsreaktionen, XX. Über Alkindiole und Kumulene," *Chemische Berichte* 96 (1963): 1221–1228.

43. Y. Kuwatani, G. Yamamoto, M. Oda, and M. Iyoda, "Nickel-Catalyzed Dimerization of 5 Cumulenes (Hexapentaenes)," *Bulletin of the Chemical Society of Japan* 78 (2005): 2188–2208.

44. N. Islam, T. Ooi, T. Iwasawa, M. Nishiuchi, and Y. Kawamura, "Thermal Cyclotrimerization of Tetraphenyl[5]cumulene(tetraphenylhexapentaene) to a Tricyclodecadiene Derivative," *Chemical Communications* (2009): 574–576.

45. D. Khim, H. Han, K.-J. Baeg, et al., "Simple Bar-Coating Process for Large-Area, High-Performance Organic Field-Effect Transistors and Ambipolar Complementary Integrated Circuits," *Advanced Materials* 25 (2013): 4302–4308.

46. S. B. Lee, B. Kang, D. Kim, et al., "Motion-Programmed Bar-Coating Method With Controlled Gap for High-Speed Scalable Preparation of Highly Crystalline Organic Semiconductor Thin Films," *ACS Applied Materials & Interfaces* 11 (2019): 47153–47161.

Supporting Information

Additional supporting information can be found online in the Supporting Information section.